(Received 10 January 2025, Accepted 17 February 2025, Scheduled 27 February 2025)

# Terahertz Metamaterial Devices with Switchable Absorption and Polarization Conversion Based on Vanadium Dioxide

Fang Wang[1,2], Jun-Jie Cui[1], Hua Liu[1], Tao Ma[1,3,*], Xu Wang[1,4], and Yu-Fang Liu[1,5]

[1] *College of Electronic and Electrical Engineering, Henan Normal University, Xinxiang 453007, China*
[2] *Key Laboratory of Optoelectronic Sensing Integrated Application, Xinxiang 45007, China*
[3] *Henan Key Laboratory of Optoelectronic Sensing Integrated Application, Xinxiang 453007, China*
[4] *The Academician Workstation of Electromagnetic Wave Engineering of Henan Province Henan Normal University, Xinxiang 453007, China*
[5] *Henan Academy of Sciences, Zhengzhou 450052, China*

**ABSTRACT:** This paper presents a switchable terahertz metamaterial device based on vanadium dioxide ($VO_2$). By leveraging its phase transition properties, the device achieves broadband absorption and polarization conversion functionality through the insulator-to-metal transition (IMT) induced by temperature modulation. When $VO_2$ is metallic, the device functions as a broadband absorber achieving an absorption rate exceeding 90% within the frequency range of 2.2 to 4.4 THz. Conversely, when $VO_2$ is in its insulating state, the device enables polarization conversion of incident terahertz waves. Simulation results reveal that in this state, the cross-polarized reflection coefficient ($R_{yx}$) exceeds 0.8, while the co-polarized reflection coefficient ($R_{xx}$) is significantly suppressed, indicating efficient conversion from co-polarization to cross-polarization within the 1.4 to 2.1 THz range. Notably, the polarization conversion rate approaches unity in this frequency band. Additionally, the study investigates the influence of the structure's geometric parameters, incident angle, and polarization angle on its performance. The results demonstrate that the device exhibits robust tolerance to variations in these parameters, as well as low manufacturing precision requirements. The proposed multifunctional switchable terahertz metamaterial device holds significant potential for applications in terahertz research, polarization filtering, and terahertz invisibility technologies.

## 1. INTRODUCTION

Terahertz waves, occupying the electromagnetic spectrum between infrared light and microwaves with frequencies ranging from 0.1 to 10 THz [1], have garnered significant attention in recent years due to the rapid advancements in optoelectronics technology. These waves demonstrate immense potential across a wide range of applications, including communication, sensing, imaging, medicine, and non-destructive testing [2]. However, the development of materials capable of effectively manipulating terahertz waves remains a challenge, due to the limited availability of natural materials with suitable properties. To address this issue, researchers have engineered a new class of artificial materials — metamaterials — which exhibit unique electromagnetic properties not found in nature.

Metamaterials [3] represent a novel class of artificially synthesized materials, composed of periodically arranged electromagnetic resonant units, exhibiting physical phenomena and characteristics not found in natural materials. Owing to their light weight, low cost, and ease of fabrication, metamaterials have found extensive applications in infrared imaging [4], energy harvesting [5], electromagnetic cloaking [6], sensors, and modulators [7, 8]. Consequently, researchers have conducted substantial studies on terahertz devices, proposing applications such as terahertz absorbers [9, 10] and polarization converters [11–13]. Previous research often featured singular functionalities with post-fabrication structural rigidity, severely limiting practical applications. Presently, most terahertz metamaterial designs demonstrate singular functions. Therefore, to expand the applications of metamaterial devices, functional materials like graphene, vanadium dioxide ($VO_2$), and GeSbTe are integrated with metamaterials, leveraging their tunable properties to achieve adjustability or reconfigurability in metamaterials. In comparison to alternative phase change materials, $VO_2$, as a phase-change material, undergoes rapid phase transitions, with conductivity changes spanning 4–5 orders of magnitude [10]. These transitions can be controlled by simple conditions such as temperature and electric field. Thus, $VO_2$ has begun to see widespread use in metamaterials and various reconfigurable devices.

To date, most metamaterials have been able to achieve a single function. Although various structures of terahertz absorbers and polarization converters based on metamaterials have emerged, these designs often suffer from complex structures and difficult tuning issues. Li et al. have proposed a multifunctional terahertz metamaterial based on nanoimprinting that achieves broadband absorption with an absorption rate of over 80% in the range of 0.82 THz to 0.93 THz. Additionally, within the 1.16 THz range, the material exhibits a transmittance rate of over 80% [14]. Wu et al. introduced a ring-shaped, ultra-wideband tunable metamaterial perfect absorber, achieving terahertz absorption rates as high as 90% in the 2.34 to 5.64 THz frequency range [15]. Fang et al. presented a dual-mode tunable

* Corresponding author: Tao Ma (matao@htu.edu.cn).

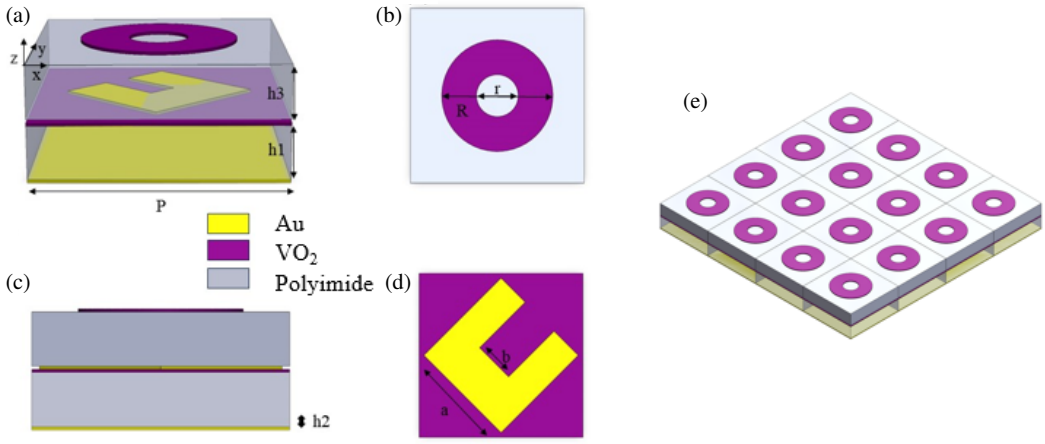


**FIGURE 1**. Schematic diagram of the designed switchable metamaterial, (a) (e) 3D schematic view and (b) (d) schematic of Pattern layers, (c) side view.

polarization conversion metasurface combining graphene and vanadium dioxide ($VO_2$), which, when $VO_2$ is in its insulating state, enables significant asymmetric transmission (AT) at 0.42 and 0.77 THz. Conversely, when $VO_2$ is metallic, the converter switches to reflection mode, exhibiting broadband polarization conversion for both forward and backward incidences. Additionally, the conductivity of graphene can be modulated by changing the gate voltage, thus achieving dynamic control of the polarization conversion bandwidth in reflection mode and asymmetric transmission in transmission mode [16].

This study leverages the phase transition properties of vanadium dioxide ($VO_2$) to propose a functionally switchable terahertz metamaterial device capable of broadband absorption and cross-polarization conversion. When $VO_2$ is in its metallic state, the device operates as a broadband absorber. Its structure consists of a bottom-to-top arrangement of a $VO_2$ film, a U-shaped metal layer, a polyimide (PI) dielectric layer, and an upper layer of $VO_2$ rings. Conversely, when $VO_2$ is in its insulating state, the device functions as a polarization converter. In this mode, the active components include upper $VO_2$ rings, an upper PI dielectric layer, U-shaped metal, $VO_2$ film, a lower PI dielectric layer, and a bottom metal substrate. Furthermore, the study systematically investigates the influence of structural parameters, incident angle, and polarization angle on the device's absorption and polarization conversion performance. Compared to traditional materials and static metamaterials, the proposed $VO_2$-based switchable metamaterial offers significant advantages, including dynamic tunability, multifunctional integration, and flexible design freedom. Leveraging the phase transition properties of $VO_2$, the device achieves seamless switching between broadband absorption and polarization conversion, which is challenging to realize with conventional approaches. This design not only enhances the functionality of terahertz devices but also provides a versatile platform for applications in communication, imaging, and sensing.

The schematic diagram and specific parameters of the metamaterial unit structure in this article are shown in Figure 1. The metamaterial cell structure is composed, from bottom to top, of a bottom metal substrate, PI (with $\varepsilon\text{PI} = 3.5 + 0.00945\text{i}$) [16], $VO_2$ film, U-shaped metal, PI, and ring-shaped $VO_2$. Through simulation and optimization analysis, the obtained optimal parameters are $P = 50\,\mu\text{m}$, $R = 16\,\mu\text{m}$, $r = 6\,\mu\text{m}$, $a = 31.25\,\mu\text{m}$, $b = 12.5\,\mu\text{m}$, $h_1 = h_3 = 10.5\,\mu\text{m}$, and $h_2 = 0.6\,\mu\text{m}$. The thicknesses of the $VO_2$ ring patch, U-shaped metal, and bottom metal substrate (with $\sigma\text{Au} = 4.561 \times 10^7$ S/m) are 0.1 μm, 0.6 μm, and 0.6 μm, respectively.

In this study, simulations are performed using the commercial software COMSOL Multiphysics. Periodic boundary conditions are applied in the $x$ and $y$ directions to model the infinite periodic nature of the structure, while perfectly matched layers (PMLs) were used in the $z$ direction to absorb outgoing waves and minimize reflections, ensuring accurate simulation results. The incident wave propagated through the entire structure in the $-z$ direction, and numerical simulations were conducted for the structure in the 0.8 to 7 THz frequency range. At terahertz frequencies, the optical dielectric constant of $VO_2$ can be described by the Drude mode [17]: $\varepsilon(\omega) = \varepsilon_\infty - \omega^2\rho(\sigma)/(\omega^2 + \text{i}\gamma\omega)$, where $\varepsilon_\infty = 12$ represents the high-frequency dielectric constant; $\omega_\rho(\sigma)$ denotes the plasma frequency related to conductivity; and $\gamma$ represents the collision frequency. In addition, a positive relationship between $\omega_\rho^2$ and $\sigma$ ($\omega_\rho^2 = \sigma/\sigma_0\omega^2\rho(\sigma_0)$) can be used to represent the plasma frequency at $\sigma$, where $\sigma_0 = 3 \times 10^2\,\Omega^{-1}\text{cm}^{-1}$, $\omega\rho(\sigma_0) = 1.4 \times 10^{15}$ rad/s, $\gamma = 5.57 \times 10^{13}$ rad/s. Set the relative permittivity of insulating $VO_2$ to 12. The phase transition process of $VO_2$ shows significant changes in conductivity and permittivity [18]. In our study, $VO_2$ conductivities of $2 \times 10^5$ S/m and 20 S/m were selected to define the metal state and insulation state, respectively [19]. These two numerical values were used to simulate the phase transition process of $VO_2$.

## 2. RESULTS AND DISCUSSIONS

### 2.1. When Vanadium Dioxide ($VO_2$) Is in Its Metallic Phase, the Proposed Switchable Metamaterial Operates as a Broadband Absorber

As illustrated in Figure 2, when the conductivity of $VO_2$ reaches $2 \times 10^5$ S/m, indicating a metallic state, the proposed switchable metamaterial device functions as a broadband ab-

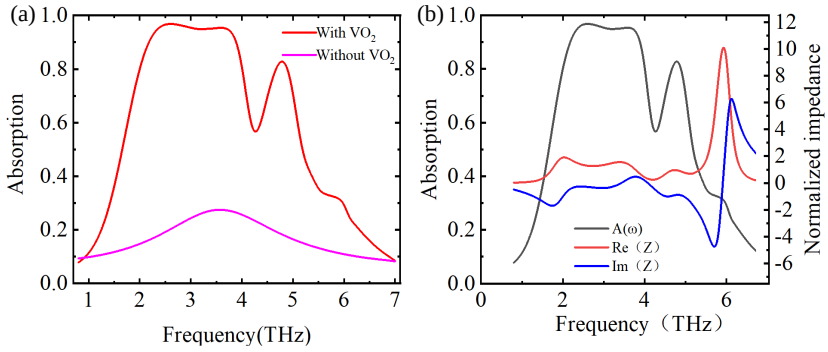


**FIGURE 2**. (a) Absorption of the designed metamaterial device with $VO_2$ patches and without $VO_2$ patches. (b) Plots of relative impedance and absorption curves.

sorber. During the simulation analysis, the finite element analysis method was employed to investigate the absorptive properties of the metamaterial device. The terahertz absorption rate of the device can be expressed by the formula derived from the simulated reflection absorption ($S_{11}$) and transmission coefficient ($S_{21}$):

$$A = 1 - R - T = 1 - |S_{11}|^2 - |S_{21}|^2 \tag{1}$$

The reflectance is denoted by $R = |S_{11}|^2$, which is derived from the parameters, while the transmittance is represented by $T = |S_{21}|^2$. In the studied terahertz frequency range, the transmission ($T$) of the designed metamaterial device is always 0 owing to the existence of metal plates or metallic $VO_2$ films at the bottom in both states, and the thickness of the metal plates or $VO_2$ films is much larger than the skin depth of terahertz waves, leading to suppressed transmission. Consequently, the terahertz absorption rate of the device can be further expressed by the following formula:

$$A = 1 - R - T = 1 - |S_{11}|^2 \tag{2}$$

The intrinsic mechanism behind the absorption characteristics of the metamaterial is studied using impedance matching theory. By employing the $S$-parameter retrieval method, the real and imaginary parts of the relative impedance of the metamaterial structure are calculated. The absorption rate and relative impedance can be expressed as [17, 20]:

$$A(\omega) = 1 - R(\omega) = 1 + \left|\frac{Z - Z_0}{Z + Z_0}\right|^2 = 1 - \left|\frac{Z_r - 1}{Z_r + 1}\right|^2 \tag{3}$$

$$Z_r = \pm\sqrt{\frac{(1 + S_{11}(\omega)^2 - S_{21}(\omega)^2)}{(1 - S_{11}(\omega)^2 - S_{21}(\omega)^2)}} \tag{4}$$

In the given formula, $Z_0$ and $Z$ represent the effective impedance of free space and the effective impedance of the structure, respectively. The relative impedance of the structure to free space is denoted by $Z_r = Z_0/Z$. According to impedance matching theory, when the impedance of the metamaterial structure matches that of free space, the absorption rate of the metamaterial absorber reaches its maximum value (at this point, the relative impedance $Z_r = 1$). Figure 2(a) illustrates the absorption rates with and without the annular $VO_2$ patch. It is evident that the introduction of the annular $VO_2$ patch significantly enhances the overall absorption rate and bandwidth. Without the $VO_2$ patch, the overall absorption rate is only about 0.2, whereas with the $VO_2$ patch, the peak absorption rate approaches 1. Notable absorption peaks are observed at 2.6 THz and 3.5 THz, with the absorption rate exceeding 90% in the frequency range of 2.2 to 3.9 THz. The bandwidth ratio can be expressed as $(f_{max} - f_{min})/[(f_{max} + f_{min})/2]$, where $f_{max}$ and $f_{min}$ represent the maximum and minimum frequencies with an absorption rate greater than 90%, respectively. The calculated bandwidth ratio is 66.7%.

In Figure 2, we compare the absorption rates with and without the $VO_2$ annular patch to illustrate its impact on the overall absorption performance. The annular $VO_2$ patch further enhances the absorption performance by optimizing the distribution of the electromagnetic field and improving impedance matching with free space. The presence of the annular patch increases the overall absorption rate and bandwidth, as demonstrated in Figure 2(a). As demonstrated in Figure 2(b), the relative impedance of the structure is matched with the impedance of free space. Within the range of 2.2 to 3.9 THz; the real part of the impedance approaches 1; and the corresponding imaginary part approaches 0, resulting in high absorption within this frequency band.

In pursuit of the optimal parameters for the metamaterial structure, a study was conducted on the geometric dimensions of the metamaterial, such as period $P$ and the inner radius of the annulus ($r$). Figure 3 illustrates the investigation into how these structural parameters affect the metamaterial's absorption rate.

As shown in Figure 3(a), an initial simulation analysis was conducted on the periodicity $P$ of the metamaterial. When $P$ is greater than 50 µm, an increase in $P$ results in a decrease in the overall absorption bandwidth, a reduction in the absorption rate at the first peak, and a slight increase at the second peak. Conversely, when $P$ is less than 50 µm, a decrease in the periodicity $P$ leads to a slight increase in the overall bandwidth. Considering the manufacturing difficulties associated with excessively small dimensions, a periodicity of $P = 50$ µm was selected for continued simulation studies. Subsequently, the impact of the annulus inner diameter $r$ on the absorption rate was simulated. As depicted in Figure 3(b), when $r > 6$ µm, an increase in $r$

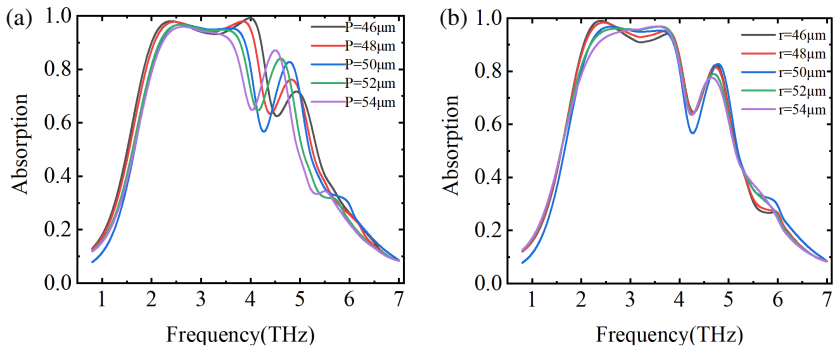


**FIGURE 3**. The absorption spectrum varies with (a) the period of $P$, (b) the radius of $r$ in the upper $VO_2$ patch.

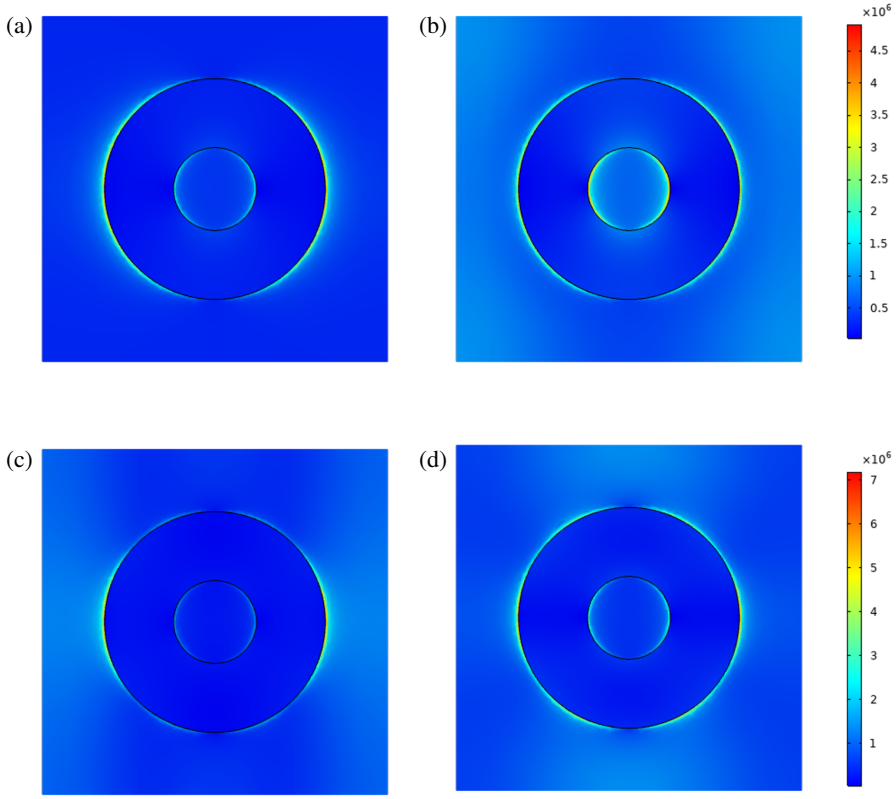


**FIGURE 4**. The absorption spectrum varies with (a) $f = 2.5$ THz, (b) $f = 3.6$ THz, (c) $f = 4.3$ THz, (d) $f = 4.8$ THz.

shows a downward trend in the overall absorption rate. When $r < 6$ μm, a decrease in $r$ slightly increases the absorption rate at the first peak, followed by a reduction after the first peak. Similarly, to avoid manufacturing challenges due to very small metamaterial dimensions, an inner diameter of $r = 6$ μm was chosen for the study. In summary, the optimal absorption rate is achieved when the parameters are set to $P = 50$ μm and $r = 6$ μm.

To gain a deeper understanding of the working mechanism of the absorber, Transverse Electric (TE) polarized terahertz waves were utilized. The electric field distribution on the surface of the top $VO_2$ annulus was studied at frequencies of 2.5 THz, 3.6 THz, 4.3 THz, and 4.8 THz, as illustrated in Figure 4.

The influence of geometric parameters, such as the dimensions of the $VO_2$ rings and the shape of the U-shaped metal structure, on the device's performance can be attributed to their impact on the resonant frequency and electromagnetic field distribution. For instance, increasing the radius of the $VO_2$ rings shifts the resonant frequency, thereby altering the absorption and polarization conversion characteristics. To better comprehend the physical mechanism of vanadium dioxide ($VO_2$) as an absorber in its metallic state, the electric field distribution at several peak frequencies during the incidence of the wave was analyzed. As indicated by Figure 4, the electric field is primarily concentrated on the inner and outer sides of the $VO_2$ annulus. In its metallic state, the $VO_2$ in the middle layer has a thickness greater than the skin depth. The incidence of electromagnetic waves on the $VO_2$ annular surface induces local-

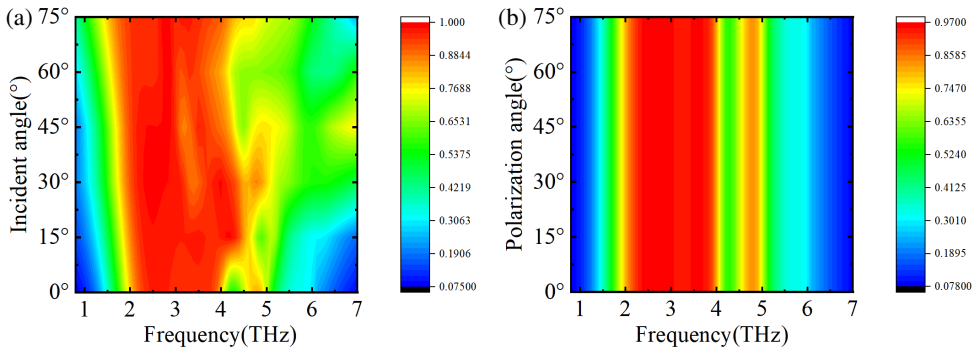


**FIGURE 5**. (a) Absorption rate of broadband absorption with diverse incident angles. (b) Absorption spectra of the wide-band absorber with different polarization angles when $\sigma = 2 \times 105$ S/m.

ized surface plasmon resonance (SPR), which causes the accumulation of electric charges to form electric dipoles. Multiple electric dipole resonances and coupling between adjacent units result in peak absorption. The broadband absorption effect is caused by superposition of resonances. As shown in Figure 4, at frequencies of $f = 2.5$ THz, $f = 3.6$ THz, and $f = 4.8$ THz, the absorption rate is high, with the electric field focused on the inner and outer sides of the annulus. However, at $f = 4.3$ THz, as depicted in Figure 4(c), the electric field is mainly distributed at the left and right ends of the outer side of the annulus, resulting in a weaker surface plasmon resonance and, consequently, a lower absorption rate at this frequency.

Finally, with practical applications in mind, the effects of the incidence angle and polarization angle on the performance of the absorber were studied. Figure 5(a) depicts the relationship between the absorption rate and incidence angle. The designed absorber maintains a stable absorption rate with a large tolerance for the incidence angle, retaining good performance even at an incidence angle of 75°. Within the broad range of 0° to 75° incidence angles, the absorption peaks exhibit a redshift as the incidence angle increases. Figure 5(b) presents the impact of the polarization angle on the absorption performance when terahertz waves impinge perpendicularly on the metamaterial structure. Due to the symmetry of the structure, the absorption rate remains almost unchanged within the range of 0° to 75° polarization angles, indicating polarization independence. The absorber's simple structure and large tolerance for incidence and polarization angles make it suitable for electromagnetic shielding to block terahertz radiation in devices. It also holds promise for enhancing image contrast and improving image quality in terahertz imaging applications.

### 2.2. When $VO_2$ Is in the Insulating State, the Proposed Switchable Metamaterial Operates as a Broadband Cross-Polarization Converter in the 1 to 3 THz Frequency Band

Based on the fundamental theory of electromagnetic waves, the components of a linearly polarized wave in two orthogonal directions differ by 0° or 180° [21]. Decomposing the electric field vector of the incident electromagnetic wave according to the uov coordinate system, if the amplitudes of the co-polarized reflection in the two orthogonal components are equal, and the phase difference is 180°, a 90° phase shift can be achieved, resulting in a polarization conversion from coplanar to cross-polarization. For an $x$-polarized electromagnetic wave incident perpendicularly, if the $x$-polarized wave is converted to a $y$-polarized wave after reflection, then the reflected electromagnetic wave through the terahertz polarization converter will have a phase difference in the $u$ and $v$ directions ($\Delta\varphi = |\varphi_{uv} - \varphi_{uu}|$). When the phase difference is approximately 180°, and $R_{uu} \approx R_{uv}$, the incident $x$-polarized wave is rotated by 90° after reflection by the polarization converter and is reflected back as a $y$-polarized wave. To understand the working principle of the designed metasurface as a linear polarizer, the electric field component along the $y$-axis can be decomposed into two orthogonal $u$ and $v$ components, with reference to the $x$ and $y$ axes at ±45° [22]. A $y$-polarized incident electromagnetic wave can be divided into $u$ and $v$ components, as shown in Figure 7(a). The metasurface exhibits anisotropy along the $u$ and $v$ axes, with mirror symmetry along the $u$ axis. We studied the incident and reflected electric fields along the $u$ and $v$ axes, denoted by $E_{ui}$ and $E_{vi}$, $E_{ur}$, and $E_{vr}$, respectively. After decomposing the incident and reflected electric fields into $u$ and $v$, they can be expressed as [23–25]:

$$E_i = uE_{ui} + vE_{vi} \tag{5}$$

$$E_r = uR_{uu}E_{ui} + vR_{vv}E_{vi} \tag{6}$$

In the formula, when the incident electromagnetic wave is $u$-polarized and $v$-polarized, the reflected polarization components are denoted by $R_{uu}$ and $R_{vv}$, respectively.

The polarization conversion ratio (PCR) refers to the efficiency with which an electromagnetic wave transitions from one polarization state to another. The PCR is defined as [26–28]:

$$PCR = \frac{|R_{yx}|^2}{|R_{yx}|^2 + |R_{xx}|^2} \tag{7}$$

In the formula, $R_{xx}$ represents the co-polarized reflection coefficient, while $R_{yx}$ denotes the cross-polarized reflection coefficient.

Additionally, it is defined that $\Delta\varphi = \varphi_{xx} - \varphi_{yx}$, the phase difference $\Delta\varphi = 2k\pi \pm \frac{\pi}{2}$ is an integer multiple of $k$ (where $k$ is an integer), and the reflected wave will be converted into a circularly polarized wave [29, 30].

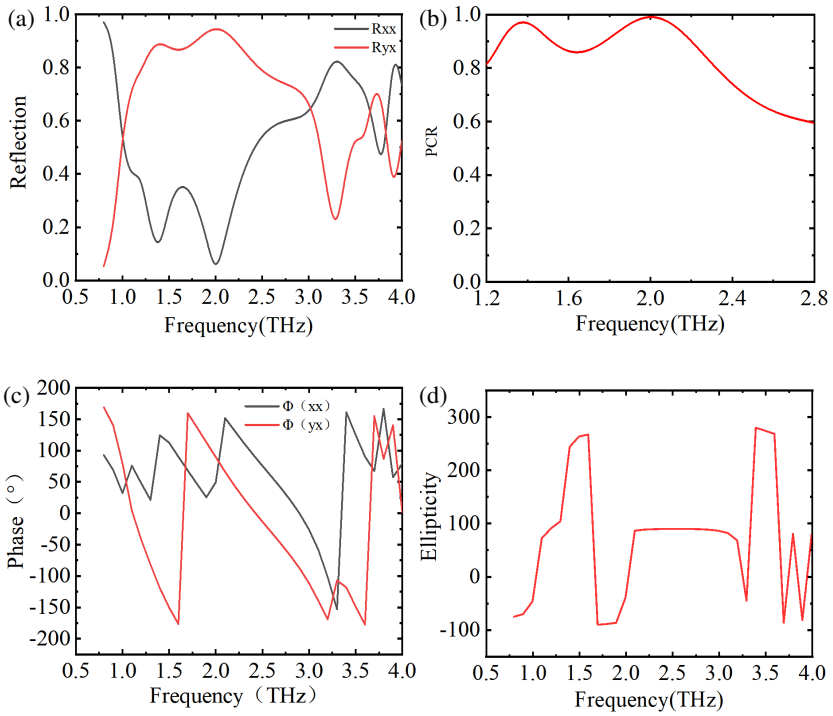


**FIGURE 6**. (a) Reflection curve. (b) Polarization conversion rate when $\sigma = 20$ S/m. (c) Phase. (d) Phase difference.

Figure 6 presents the simulated reflection coefficients and PCR for a linearly polarized wave incident perpendicularly on the broadband polarization converter. As can be seen from Figure 6(a), within the frequency range of 1.4–2.5 THz, the cross-polarized reflection coefficient $R_{yx}$ is above 0.8, achieving the planned conversion functionality. Figure 6(b) reveals that within the frequency range of 1.4–2.3 THz, the cross-linear polarization conversion efficiency exceeds 80%, and within 1.4–2.1 THz, it approaches 1, enabling a near-perfect cross-polarization conversion. Under the condition of $|R_{yx}| = |R_{xx}|$ [31, 32], it is known from Figure 6(d) that at frequencies of 1–1.1 THz, $\Delta\varphi$ is approximately $-90°$, and at frequencies of 2.1–3 THz, $\Delta\varphi$ is about 90°. At frequencies of 1–1.1 THz and 3.0–3.2 THz, the linearly polarized wave can be converted into a circularly polarized wave.

To better analyze the mechanism behind polarization conversion, the current density of the gold structure layer and gold substrate layer was examined at 2 THz. Figures 7(c) and 7(d) illustrate the decomposition of the current components ($P_1$, $P_2$, and $P_3$) in the upper and lower layers at 2 THz. It is observed that the $x$-component of $P_1$ ($P_{1x}$) is opposite in direction to $P_2$ and the $x$-component of $P_3$ ($P_{3x}$), which couple to form an electromagnetic resonance. This resonant interference superposition endows the metamaterial with wide-band polarization conversion properties.

Subsequently, to identify the optimal parameters for the metamaterial structure, a parametric study was conducted on its geometric dimensions, including the period ($P$), gap width ($b$), side length ($a$), and the thickness of $VO_2$ ($h_2$). Figure 8 demonstrates the influence of these dimensional parameters on the metamaterial's polarization conversion rate.

Figure 8(a) illustrates the relationship between the polarization conversion ratio (PCR) and the periodicity $P$ of the metamaterial when other parameters remain constant. As $P$ increases from 46 μm to 54 μm, the overall resonance peaks redshift towards lower frequencies, and the PCR slightly decreases. Considering the manufacturing difficulties associated with very small dimensions, a periodicity of $P = 50$ μm was chosen to achieve a relatively optimal PCR size. Figure 9(b) demonstrates the relationship between the PCR and gap width $b$ when other parameters are unchanged. As the gap width increases by 0.5 μm from 11.5 μm to 13.5 μm, the PCR tends to decrease at lower frequencies and gradually increases at higher frequencies. Taking into account this variation, a gap width of $b = 12.5$ μm was selected. Figure 9(c) investigates the effect of $a$ (the U-shaped metal bottom side length, which is shown in Figure 1(d)) on the PCR. When $a = P/1.5$, the overall PCR is relatively low; when $a = P/1.6$, the PCR is close to 1; however, the frequency range is narrower. As the size of $a$ decreases, the conversion efficiency gradually decreases, hence $a = P/1.6$ was chosen. Figure 8(d) examines the impact of the $VO_2$ thickness $h_2$ on the PCR, indicating that the thickness of $h_2$ has almost no effect on the PCR.

The angle of terahertz waves significantly influences the polarization conversion characteristics of metamaterials. To evaluate the angular stability of the polarization converter, simulations are performed to analyze the effects of variations in the incidence angle and polarization angle on its performance. Figure 9 illustrates the impact of these angular variations on the polarization conversion efficiency (PCR). As shown in Figure 9(a), as the incidence angle increases from 0° to 45°, the PCR exhibits a slight decrease in the low-frequency range and

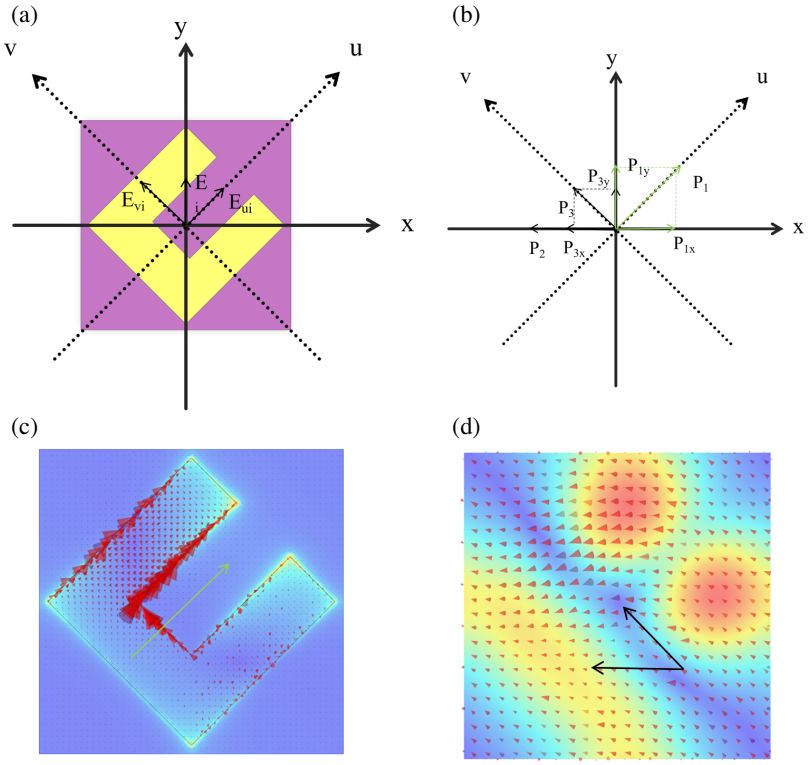


**FIGURE 7**. (a) Polarized electric field decomposed into $u$ and $v$. (c) (d) The surface current density of gold structure layer and gold substrate layer at 2 THz.

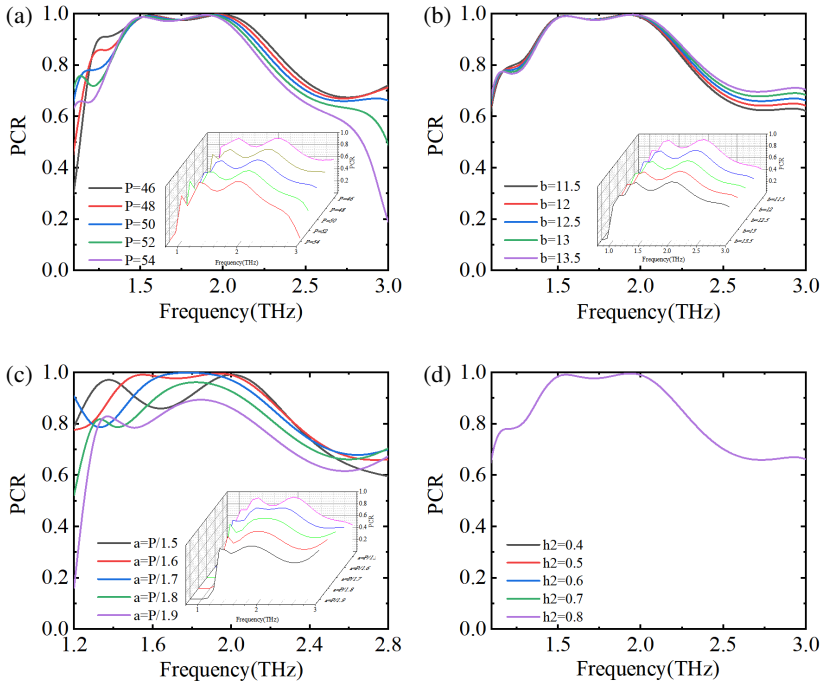


**FIGURE 8**. The influence of structural parameters on polarization conversion rate (a) $P$, (b) $b$, (c) $a$, (d) $h_2$.

a slight increase in the high-frequency range. This behavior indicates that the device maintains robust performance across a wide range of incidence angles (0°–45°). Figure 9(b) demonstrates that the PCR remains nearly constant with increasing polarization angle, which is attributed to the symmetric design of the metamaterial device, making it insensitive to polarization angle variations.

Due to its excellent angular stability and polarization conversion performance, the proposed device holds significant potential for applications in terahertz radar systems. By controlling

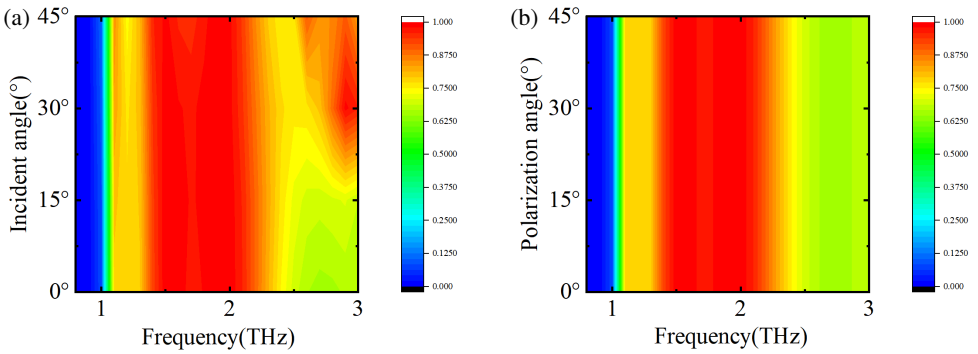


**FIGURE 9**. (a) PCR with diverse incident angles and (b) PCR with different polarization angles.

**TABLE 1**. Comparison of the present MMA with others.

| Ref. | Material | Frequency (THz) | Absorption | Polarization converter | Flexible |
|---|---|---|---|---|---|
| [33] | PI, copper | 0.72, 1.4, 2.3 | 89%, 98%, 85% | no | yes |
| [34] | $VO_2$, mica, gold | 0.24, 0.46 | 99.7%, 99.3% | no | no |
| [35] | $VO_2$, mica, gold | no | No | 0.4–1.1 THz | yes |
| [20] | $VO_2$, $SiO_2$, Graphene | 0.98–1.63 | Above 90% | no | yes |
| [36] | Graphene, $VO_2$ | 0.7, 2.1, 3.9 and 0.8–2.4 | Above 90% | no | no |
| Our paper | $VO_2$, PI, gold | $2.2 \sim 4.4$ | Above 90% | $1.4 \sim 2.5$ THz | yes |

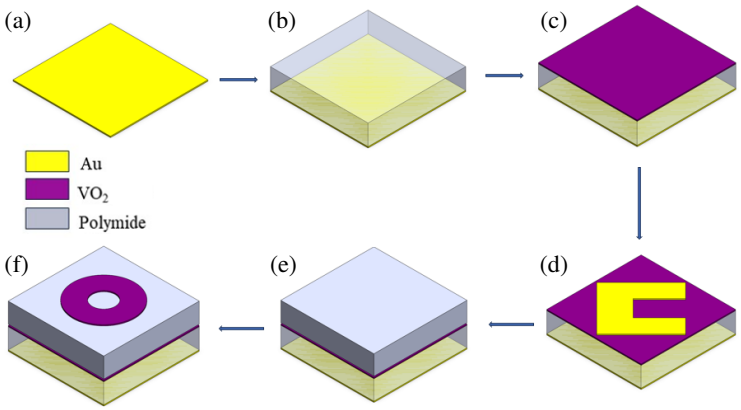


**FIGURE 10**. Proposed potential manufacturing processes for terahertz switchable metamaterials.

the polarization of emitted electromagnetic waves, the device can extract polarization information from targets, thereby enhancing target recognition and imaging capabilities. Additionally, the polarization converter can be utilized in terahertz communication systems, where signal polarization adjustment can optimize transmission efficiency and mitigate interference.

Table 1 provides a comparison of our proposed structure with several previously published works. Our results show that, compared to existing designs, our structure offers a simpler yet highly versatile solution capable of multifunctional switching. Furthermore, it exhibits low manufacturing process requirements and robust performance stability under variations in incidence angle and polarization angle. These advantages make the proposed structure highly promising for practical applications requiring consistent and reliable performance.

### 2.3. Terahertz Metamaterial Device Manufacturing Process

The proposed metamaterial is designed for the ease of fabrication [3, 37, 38] with the manufacturing process illustrated in Figure 10. The specific steps are as follows: (a) Gold Film Deposition: A gold film is electroplated onto a silicon substrate. The substrate is first cleaned, and an adhesion layer (e.g., chromium or titanium) is deposited to ensure strong bonding. The gold film is then electroplated to a thickness of several hundred nanometers, ensuring uniform coverage. (b) Polyimide Dielectric Layer: A polyimide dielectric layer is spin-

coated onto the gold film and cured at high temperatures (300–350°C), forming a stable dielectric layer several micrometers thick. (c) $VO_2$ Thin Film: A $VO_2$ thin film is deposited onto the polyimide surface using magnetron sputtering and patterned via photolithography. Photoresist is applied, exposed, and developed, followed by etching to achieve the desired $VO_2$ pattern. (d) U-shaped Metal Layer: The U-shaped metal layer is fabricated through photolithography and metallization. Photoresist is spin-coated and patterned via exposure, after which a metal layer (e.g., gold or aluminum) is deposited. The resist is then lifted off to form the U-shaped structure. (e) Additional Polyimide Layer: Another polyimide dielectric layer is spin-coated and cured, covering the U-shaped metal structure to ensure uniformity and stability. (f) $VO_2$ Annular Layer: A $VO_2$ thin film is deposited onto the polyimide layer using magnetron sputtering and patterned via photolithography to form an annular structure.

This detailed fabrication process ensures the precise construction of the proposed metamaterial, enabling its unique functional properties and performance.

## 3. CONCLUSION

In summary, leveraging the phase transition properties of $VO_2$, this paper proposes a switchable terahertz metamaterial device. Through simulation analysis and optimization of geometric parameters, it is demonstrated that this multifunctional switchable metamaterial can act as a terahertz absorber and polarization converter. When $VO_2$ is metallic, this multifunctional device can be used as a broadband absorber. The results show that in the $2.2 \sim 4.4$ THz frequency range, the absorption rate exceeds 90%. When $VO_2$ is an insulator, the structure serves as a polarization converter. In this state, within the $1.4 \sim 2.5$ THz frequency range, simulation results show that reflection coefficients $R_{xx}$ and cross-polarized reflection coefficients $R_{yx}$ are observed, with with $R_{yx}$ being the cross-polarized reflection coefficient greater than 0.8. In the $1.4 \sim 2.1$ THz frequency range, the polarization conversion rate is close to 1. At frequencies of 1–1.1 THz and 3.0–3.2 THz, linearly polarized waves can be converted into circularly polarized waves. The designed metamaterial structure is simple, with switchable functionality. Moreover, the properties of the metamaterials were simulated at various sizes, revealing their remarkable tolerance to dimensional variations. This high tolerance ensures that manufacturing errors have minimal impact on the performance and functionality of the metamaterials. As a result, the device is suitable for a wide range of applications including electromagnetic shielding, terahertz imaging, and terahertz communication.

## ACKNOWLEDGEMENT

The National Natural Science Foundation of China (NSFC) (62075057 and 62075058).

## DECLARATION OF INTERESTS

The authors declare that they have no known competing financial interests or personal relationships that could have appeared to influence the work reported in this paper.

## REFERENCES

[1] Qiu, Y., D.-X. Yan, Q.-Y. Feng, X.-J. Li, L. Zhang, G.-H. Qiu, and J.-N. Li, "Vanadium dioxide-assisted switchable multifunctional metamaterial structure," *Optics Express*, Vol. 30, No. 15, 26 544–26 556, 2022.

[2] Tao, Y. H., A. J. Fitzgerald, and V. P. Wallace, "Non-contact, non-destructive testing in various industrial sectors with terahertz technology," *Sensors*, Vol. 20, No. 3, 712, 2020.

[3] Nagini, K. B. S. S. and D. S. Chandu, "Terahertz wideband cross-polarization conversion metasurface based on double split-ring resonator," *AEU — International Journal of Electronics and Communications*, Vol. 170, 154826, 2023.

[4] Qin, Z., D. Meng, F. Yang, X. Shi, Z. Liang, H. Xu, D. R. Smith, and Y. Liu, "Broadband long-wave infrared metamaterial absorber based on single-sized cut-wire resonators," *Optics Express*, Vol. 29, No. 13, 20 275–20 285, 2021.

[5] Lu, Z.-Q., L. Zhao, H. Ding, and L.-Q. Chen, "A dual-functional metamaterial for integrated vibration isolation and energy harvesting," *Journal of Sound and Vibration*, Vol. 509, 116251, 2021.

[6] Zhao, G., S. Bi, M. Niu, and Y. Cui, "A zero refraction metamaterial and its application in electromagnetic stealth cloak," *Materials Today Communications*, Vol. 21, 100603, 2019.

[7] Liu, W., J. Xu, and Z. Song, "Bifunctional terahertz modulator for beam steering and broadband absorption based on a hybrid structure of graphene and vanadium dioxide," *Optics Express*, Vol. 29, No. 15, 23 331–23 340, 2021.

[8] Wang, J., H. Tian, Y. Wang, X. Li, Y. Cao, L. Li, J. Liu, and Z. Zhou, "Liquid crystal terahertz modulator with plasmon-induced transparency metamaterial," *Optics Express*, Vol. 26, No. 5, 5769–5776, 2018.

[9] Lan, J., R. Zhang, H. Bai, C. Zhang, X. Zhang, W. Hu, L. Wang, and Y. Lu, "Tunable broadband terahertz absorber based on laser-induced graphene," *Chinese Optics Letters*, Vol. 20, No. 7, 073701, 2022.

[10] Zhang, M., J. Zhang, A. Chen, and Z. Song, "Vanadium dioxide-based bifunctional metamaterial for terahertz waves," *IEEE Photonics Journal*, Vol. 12, No. 1, 1–9, 2020.

[11] Tang, B. and Y. Ren, "Tunable and switchable multi-functional terahertz metamaterials based on a hybrid vanadium dioxide-graphene integrated configuration," *Physical Chemistry Chemical Physics*, Vol. 24, No. 14, 8408–8414, 2022.

[12] Yang, C., Q. Gao, L. Dai, Y. Zhang, H. Zhang, and Y. Zhang, "Bifunctional tunable terahertz circular polarization converter based on dirac semimetals and vanadium dioxide," *Optical Materials Express*, Vol. 10, No. 9, 2289–2303, 2020.

[13] Zhao, Y., R. Yang, J. Wang, X. Wei, J. Tian, and W. Zhang, "Dual-mode terahertz broadband polarization conversion metasurface with integrated graphene-$VO_2$," *Optics Communications*, Vol. 510, 127895, 2022.

[14] Li, X., T. Cui, S. Zhuang, W. Qian, L. Lin, W. Su, C. Gong, and W. Liu, "Multi-functional terahertz metamaterials based on nano-imprinting," *Optics Express*, Vol. 31, No. 6, 9224–9235, 2023.

[15] Wu, G., X. Jiao, Y. Wang, Z. Zhao, Y. Wang, and J. Liu, "Ultra-wideband tunable metamaterial perfect absorber based on vana-

dium dioxide," *Optics Express*, Vol. 29, No. 2, 2703–2711, 2021.
[16] Lin, R., F. Lu, X. He, Z. Jiang, C. Liu, S. Wang, and Y. Kong, "Multiple interference theoretical model for graphene metamaterial-based tunable broadband terahertz linear polarization converter design and optimization," *Optics Express*, Vol. 29, No. 19, 30 357–30 370, 2021.
[17] Huang, J., J. Li, Y. Yang, J. Li, J. Li, Y. Zhang, and J. Yao, "Active controllable dual broadband terahertz absorber based on hybrid metamaterials with vanadium dioxide," *Optics Express*, Vol. 28, No. 5, 7018–7027, 2020.
[18] Ordonez-Miranda, J., Y. Ezzahri, K. Joulain, J. Drevillon, and J. J. Alvarado-Gil, "Modeling of the electrical conductivity, thermal conductivity, and specific heat capacity of $VO_2$," *Physical Review B*, Vol. 98, No. 7, 075144, 2018.
[19] Zhang, C., H. Zhang, F. Ling, and B. Zhang, "Dual-regulated broadband terahertz absorber based on vanadium dioxide and graphene," *Applied Optics*, Vol. 60, No. 16, 4835–4840, 2021.
[20] Zhou, R., T. Jiang, Z. Peng, Z. Li, M. Zhang, S. Wang, L. Li, H. Liang, S. Ruan, and H. Su, "Tunable broadband terahertz absorber based on graphene metamaterials and $VO_2$," *Optical Materials*, Vol. 114, 110915, 2021.
[21] Wang, B.-X., G. Duan, W. Lv, Y. Tao, H. Xiong, D.-Q. Zhang, G. Yang, and F.-Z. Shu, "Design and experimental realization of triple-band electromagnetically induced transparency terahertz metamaterials employing two big-bright modes for sensing applications," *Nanoscale*, Vol. 15, No. 45, 18 435–18 446, 2023.
[22] Wang, B.-X., X. Qin, G. Duan, G. Yang, W.-Q. Huang, and Z. Huang, "Dielectric-based metamaterials for near-perfect light absorption," *Advanced Functional Materials*, Vol. 34, No. 37, 2402068, 2024.
[23] Bai, J., T. Chen, S. Wang, W. Xu, and S. Chang, "Ultra-broadband and high-efficiency terahertz reflective metamaterials polarization converter," *Applied Physics A*, Vol. 129, No. 9, 610, 2023.
[24] Lian, M., Y. Su, K. Liu, S. Zhang, X. Chen, H. Ren, Y. Xu, J. Chen, Z. Tian, and T. Cao, "Nonvolatile switchable broadband polarization conversion with wearable terahertz chalcogenide metamaterials," *Advanced Optical Materials*, Vol. 11, No. 9, 2202439, 2023.
[25] Sun, Z., X. Wang, J. Wang, H. Li, Y. Lu, and Y. Zhang, "Switchable multifunctional terahertz metamaterials based on the phase-transition properties of vanadium dioxide," *Micromachines*, Vol. 13, No. 7, 1013, 2022.
[26] Barkabian, M., N. Sharifi, and N. Granpayeh, "Multi-functional high-efficiency reflective polarization converter based on an ultra-thin graphene metasurface in the THz band," *Optics Express*, Vol. 29, No. 13, 20 160–20 174, 2021.
[27] Cui, Z., Z. Xiao, M. Chen, F. Lv, and Q. Xu, "A transmissive linear polarization and circular polarization cross polarization converter based on all-dielectric metasurface," *Journal of Electronic Materials*, Vol. 50, 4207–4214, 2021.
[28] Yu, F.-Y., X.-J. Shang, W. Fang, Q.-Q. Zhang, Y. Wu, W. Zhao, J.-F. Liu, Q.-Q. Song, C. Wang, J.-B. Zhu, and X.-B. Shen, "A terahertz tunable metamaterial reflective polarization converter based on vanadium oxide film," *Plasmonics*, Vol. 17, No. 2, 823–829, 2022.
[29] Dai, L., L. Qi, J. A. Uqaili, Y. Zhang, H. Zhang, F. Kou, and Y. Yang, "Tunable dual-band dual-polarization terahertz polarization converter and coding metasurfaces based on Weyl semimetals," *Applied Physics B*, Vol. 129, No. 5, 81, 2023.
[30] Qiu, L.-L., S. Fang, L. Zhu, L. Deng, S. Huang, Y. Wu, X. Gao, and X. Zhang, "Wideband high-selective linear polarization converter and its application in bifunctional metasurface for reduced isolation band," *IEEE Transactions on Antennas and Propagation*, Vol. 71, No. 3, 2735–2744, 2023.
[31] Lin, X., Z. Shen, and D. Huang, "Broadband circular polarization selector and converter based on multilayer metamaterials with stacked split-rings," *Physical Review Materials*, Vol. 8, No. 1, 015203, 2024.
[32] Zhu, Y., Z. Huang, J. Su, and B. Tang, "Actively tunable and switchable terahertz metamaterials with multi-band perfect absorption and polarization conversion," *Physical Chemistry Chemical Physics*, Vol. 26, No. 15, 11 649–11 656, 2024.
[33] Liu, H., Z.-H. Wang, L. Li, Y.-X. Fan, and Z.-Y. Tao, "Vanadium dioxide-assisted broadband tunable terahertz metamaterial absorber," *Scientific Reports*, Vol. 9, No. 1, 5751, 2019.
[34] Jiang, Z., J. Leng, J. Li, J. Li, B. Li, M. Yang, X. Wang, and Q. Shi, "Flexible terahertz metamaterials absorber based on $VO_2$," *Photonics*, Vol. 10, No. 6, 621, 2023.
[35] Du, H., M. Jiang, L. Zeng, L. Zhang, W. Xu, X. Zhang, and F. Hu, "Switchable terahertz polarization converter based on $VO_2$ metamaterial," *Chinese Physics B*, Vol. 31, No. 6, 064210, 2022.
[36] Wang, G., T. Wu, J. Jiang, Y. Jia, Y. Gao, and Y. Gao, "Switchable terahertz absorber from single broadband to triple-narrowband," *Diamond and Related Materials*, Vol. 130, 109460, 2022.
[37] Dong, L., L. Si, H. Xu, Q. Shen, X. Lv, Y. Zhuang, and Q. Zhang, "Rapid customized design of a conformal optical transparent metamaterial absorber based on the circuit analog optimization method," *Optics Express*, Vol. 30, No. 5, 8303–8316, 2022.
[38] Du, Z., J. Liang, T. Cai, G. Wang, T. Deng, and B. Wu, "Designing an ultra-thin and wideband low-frequency absorber based on lumped resistance," *Optics Express*, Vol. 30, No. 2, 914–925, 2022.